Journal of Porphyrins and Phthalocyanines
J. Porphyrins Phthalocyanines 2012; **16**: 833–844
DOI: 10.1142/S1088424612500885

Published at http://www.worldscinet.com/jpp/

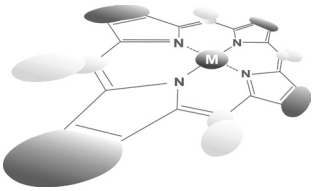

Trends in the optical and redox properties of tetraphenyltetraphenanthroporphyrins

John Mack[†a◊], Kevin Lobb[b], Tebello Nyokong[*b◊], Zhen Shen[*c◊] and Nagao Kobayashi[*a◊]

[a] *Department of Chemistry, Graduate School of Science, Tohoku University, 980-8578 Sendai, Japan*
[b] *Department of Chemistry, Rhodes University, 6140 Grahamstown, South Africa*
[c] *State Key Laboratory of Coordination Chemistry, Nanjing National Laboratory of Microstructures, School of Chemistry and Chemical Engineering, Nanjing University, Nanjing 210093, China*

Dedicated to Professor Tebello Nyokong on the occasion of her 60th birthday

Received 15 January 2012
Accepted 22 March 2012

ABSTRACT: The results of TD-DFT calculations for a series of tetraaryltetraphenanthroporphyrins containing *para*-substituents with differing electron donating and accepting properties are compared to the observed optical and redox properties and Michl's perimeter model is used as a conceptual framework for analyzing the results.

KEYWORDS: tetraphenyltetraphenanthroporphyrins, Michl's perimeter model, TD-DFT calculations, MCD spectroscopy.

INTRODUCTION

Red-shifted porphyrinoid chromophores have been the focus of considerable research interest in recent years because of their potential use as photosensitizers in photodynamic therapy (PDT) [1], as fluorescent probes for the recognition of cationic or anionic analytes [2] and as dyes for applications in nonlinear optics [3], optical limiting [4], opto-electronic devices [5] and solar energy conversion [6]. A red shift of the absorption and emission bands of porphyrins is usually achieved by expanding the π-conjugation system. A number of different approaches have been adopted in this regard over the last decade, including the introduction of *meso*-alkynyl substituents [7], an increase in the number of core pyrrole rings to form sapphyrins, hexaphyrins, octaphyrins, *etc*. [8], co-planar polymerization of porphyrins [9], the expansion of the π-system with peripheral fused rings [10, 11] and conformational distortions due to steric crowding of peripheral substituents [12, 13].

Although fused ring expansion of the ligand at the β-pyrrole positions is probably the most obvious strategy for modifying the electronic and optical properties of the π-system, only limited red shifts have been observed upon substitution with fused benzene rings [10]. Spence and Lash [14] demonstrated that the introduction of peripheral acenaphthalene rings has a significantly larger impact on the energies of the main ππ* transitions and that further red shifts are observed when phenyl substituents are added at the *meso*-carbons to form the deeply saddled tetraphenyltetraacenaphthoporphyrin (TPTANP) ligand. Shen and coworkers subsequently prepared a series of even more deeply saddled *meso*-tetraaryltetraphenanthroporphyrin (TPTP) ligands [15, 16] (Scheme 1), which resulted in a larger red shift of the Q and B bands relative to the spectra of tetraphenylporphyrin (TPP) and TPTANP. Mack *et al*. [17] demonstrated, based on an application of Michl's perimeter model [18] to the magnetic circular dichroism (MCD) spectroscopy and

◊SPP full member in good standing

*Correspondence to: Tebello Nyokong, email: t.nyokong@ru.ac.za, tel: +27 46-603-8801, fax: +27 46-622-5109; Zhen Shen, email: zshen@nju.edu.cn, tel: +86 25-8368-6679, fax: +86 25-8331-4502 and Nagao Kobayashi, email: nagaok@m.tohoku.ac.jp, tel/fax: +81 22-795-7719
†Current address: Department of Chemistry, Rhodes University, 6140 Grahamstown, South Africa

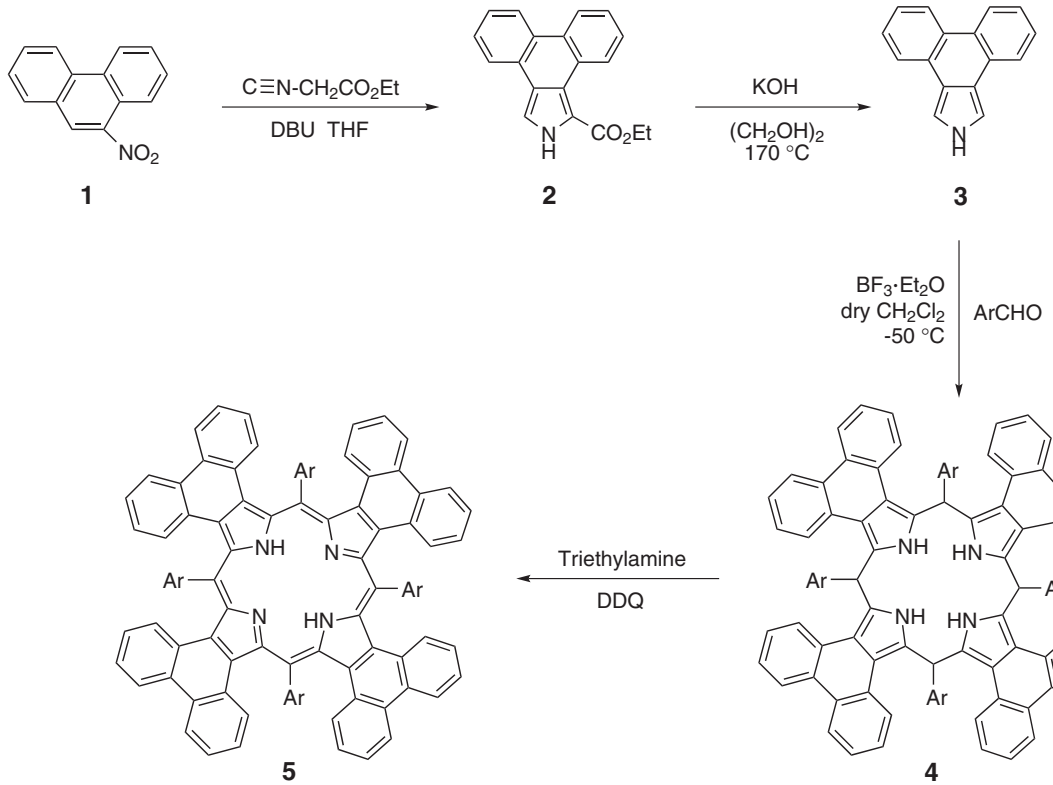

Scheme 1. Scheme for the preparation of **5a** (Ar = C_6H_5), **5b** (Ar = 4–Me–C_6H_4), **5c** (Ar = 4–F–C_6H_4), **5d** (Ar = 4–Cl–C_6H_4), **5e** (Ar = 4–Br–C_6H_4), **5f** (Ar = 4–I–C_6H_4), **5g** (Ar = 4–NC–C_6H_4), **5h** (Ar = 4–O_2N–C_6H_4) and **5i** (Ar = 4–Me_2N–C_6H_4)

theoretical calculations of seventeen radially symmetric zinc porphyrinoids, that key trends observed in the spectral properties of porphyrinoids are largely determined by the relative energies of the four frontier π-MOs associated with Gouterman's 4-orbital model [19]. Recent studies on core modified tetrabenzoporphyrins [20] and α-phenylated phthalocyanines [21] have demonstrated that the results of DFT geometry optimizations are very similar to those obtained by X-ray crystallography when steric hindrance between peripheral fused rings results in severe ligand folding due to the lack of conformational flexibility. Trends observed in the experimental data for TPTPs can, therefore, be readily compared to those predicted in theoretical calculations for B3LYP optimized geometries even in the absence of X-ray structures. In this paper the utility of TD-DFT calculations for predicting the optical and redox properties of porphyrinoid structures, which differ with regard to their peripheral fused ring and aryl *meso*-substituents, is assessed.

The deep saddling distortion of the π-system predicted in the B3LYP geometry optimization for **5i** (Fig. 1), tilts the *meso*-phenyl rings almost into the plane of the four pyrrole nitrogens facilitating conjugation between the *meso*-groups and the inner perimeter of the π-system [16]. As a result, even subtle electronic effects such as those associated with the halogen substituent series, **5c**–**5f** (Scheme 1), were found to alter the optical spectroscopy to a readily observable extent. A strong correlation was observed for the compounds with electron withdrawing substituents when the B band maxima of free base TPTPs were plotted against the Hammett parameter σ_p [16]. In this paper, a detailed analysis of TD-DFT calculations for various fused-ring-expanded porphyrinoid compounds and a series of eight TPTP compounds containing different *para*-substituents on the phenyl groups is reported, which provides further insights into the optical and redox properties of these compounds.

EXPERIMENTAL

Theoretical calculations

Theoretical calculations were carried out using the G03W software package [22] on the Perkin computer cluster in the Department of Chemistry at Rhodes University in Grahamstown, South Africa. The B3LYP functional was used with 6-31G(d) basis sets for both the geometry optimizations and the TD-DFT calculations for the fused-ring-expanded porphyrinoid compounds, **5a**–**5e** and **5g**–**5i**, while 3–21G* basis sets were used for **5f**.

ELECTRONIC STRUCTURE OF PORPHYRINOIDS

MCD spectroscopy [23] has been used to definitively identify the main electronic bands of a series of TPTPs [16].

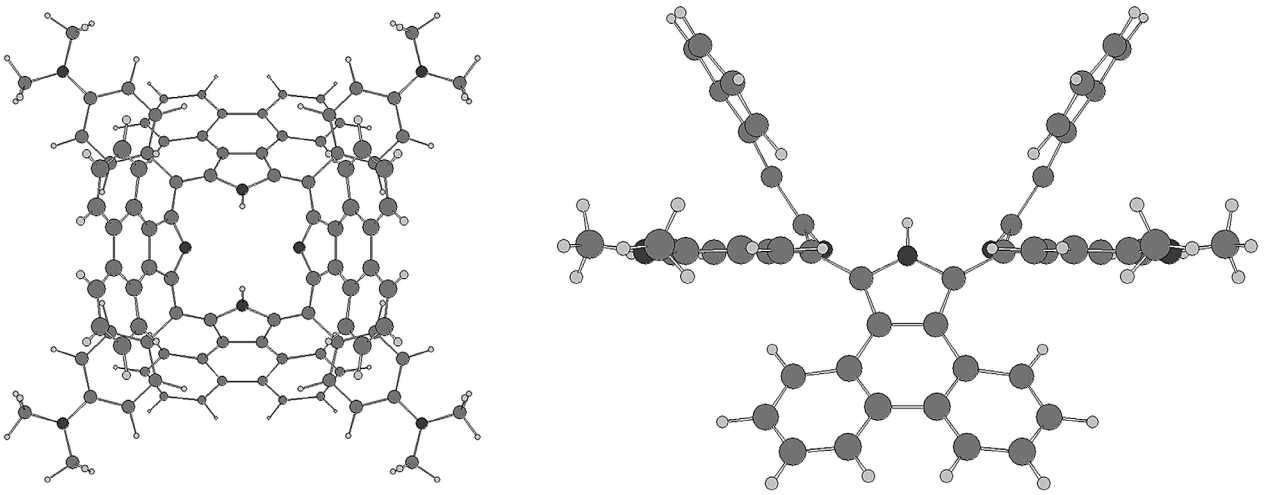

5i

Fig. 1. The B3LYP-optimized geometry of **5i** exhibit a deep saddled conformation when viewed along the *z*- (LEFT) and *y*- (RIGHT) axes

In this paper, the MCD spectral data are used to validate theoretical descriptions of the electronic structures provided by calculated TD-DFT and ZINDO/s spectra. The analysis of the MCD spectra is based on intensity mechanisms described by the Faraday $\mathcal{A}_1$, $\mathcal{B}_0$ and $\mathcal{C}_0$ terms [23]. The application of TD-DFT to the three Faraday terms is still under development so MCD spectra can not currently be calculated using commercial software packages such as the Gaussian and Amsterdam Density Functional software suites. Older theoretical approaches for describing the electronic structures of porphyrinoids, such as Gouterman's four orbital model [19] and Michl's perimeter model [18], can still be used to provide a conceptual framework for validating the results of theoretical calculations, however. Moffitt [24] and Michl [18] demonstrated that the relative intensities of the major electronic absorption bands of aromatic π-systems can be successfully described in terms of perturbations to the structure of a high-symmetry parent hydrocarbon ($C_{16}H_{16}^{2-}$ in the case of metal tetrapyrrole porphyrinoid complexes or $C_{18}H_{18}$ for free base compounds). The nodal patterns of the π-system MOs are retained even when the symmetry of the cyclic perimeter is modified. As a consequence of this there is an $M_L = 0, \pm1, \pm2, \pm3, \pm4, \pm5, \pm6, \pm7, 8$ sequence in ascending energy terms in the π-MOs of metal porphyrinoids in an analogous manner to the $M_L = 0, \pm1, \pm2, 3$ π-MO sequence that forms the basis of the aromatic properties of benzene. Within the band nomenclature of Gouterman's 4-orbital model [19], there is an electronically allowed B transition and a forbidden Q transition linking the frontier $M_L = \pm4, \pm5$ π-MOs based, respectively, on $\Delta M_L = \pm1$ and ±9 transitions. When a structural perturbation results in a marked lifting of the degeneracy of the MOs derived from the HOMO and/or LUMO of the parent perimeter (referred to as the ΔHOMO and ΔLUMO values within Michl's terminology [18]) there is a mixing of the allowed and forbidden properties of the Q and B bands and a marked intensification of the Q band, which as a consequence can become the dominant spectral feature for some porphyrinoids such as the phthalocyanines [25]. When ΔHOMO ≈ ΔLUMO the Q bands remain relatively weak, since the orbital angular momentum (OAM) properties of the parent hydrocarbon perimeter are retained and absorption intensity in the Q band region is based primarily on vibrational borrowing from the allowed B(0,0) bands [26].

Michl [18] introduced an **a**, **s**, **–a** and **–s** terminology for the four MOs derived from the HOMO and LUMO of the parent perimeter so that π-systems of porphyrinoids with differing molecular symmetry and with different relative orderings of the four frontier π-MOs in energy terms can be readily compared. One MO derived from the HOMO of the parent perimeter and another derived from the LUMO have nodal planes which coincide with the *yz*-plane and are referred to, respectively, as the **a** and **–a** MOs, while the corresponding MOs with antinodes on the *yz*-plane are referred to as the **s** and **–s** MOs. The HOMO level of 4N+2 π-electron systems have 2N nodal planes, while the LUMO levels have 2(N+1) effectively forming an octagon or a decagon on the 16 atom inner perimeter (Fig. 2). The D_{4h} symmetry of the porphyrin dianion dictates that the **–a** and **–s** MOs are degenerate since the $M_L = \pm5$ nodal patterns differ along the *x*- and *y*-axes only by being rotated by 90° with respect to each other.

RESULTS AND DISCUSSION

The B3LYP optimized geometries calculated with 6–31G(d) basis sets for **5a**–**5e**, **5g** and **5h** have geometries similar to that of **5i** (Fig. 1 and Table 1),

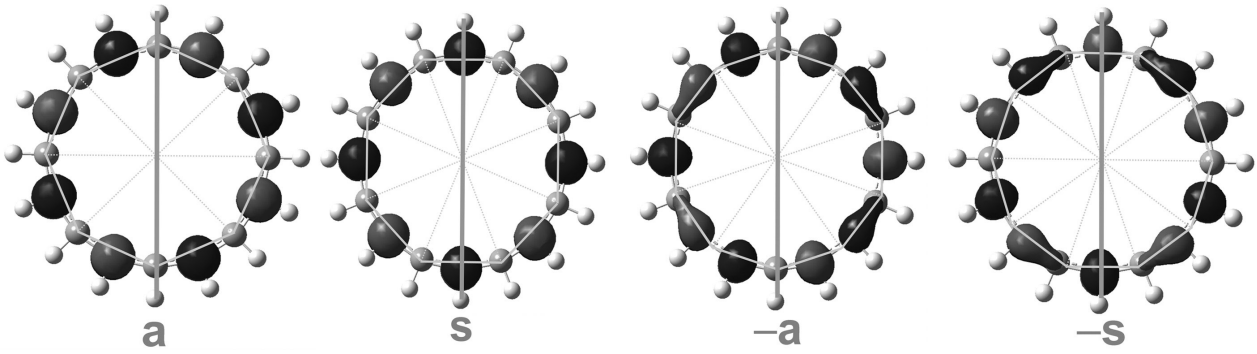

Fig. 2. In Michl's perimeter model [18] the nodal properties of the frontier π-MOs on the inner perimeter of porphyrinoid ligands can be understood based on a $C_{16}H_{16}^{2-}$ parent hydrocarbon. Gray and black are used to denote the phase changes in the isosurfaces of the MO at 0.04 a.u. The 2N nodal planes of the MOs derived from the HOMO of a 4N+2 parent perimeter typically form octagons on the perimeter with the planes running through alternating atoms, while the 2(N+1) nodal planes of the LUMO level MOs form a decagon in which the nodal planes, with the exception of those lying on either the *x*- or *y*-axis, do not coincide with atom positions. When there is a symmetry lowering perturbation such as fused ring expansion or core modification, the nodal patterns are determined by the alignment of the plane of symmetry in the *yz*-plane. Michl introduced **a**, **s**, **–a** and **–s** nomenclature to describe the four frontier π-MOs in this context based on whether there is a nodal plane (**a** and **–a**) or an antinode (**s** and **–s**) on what corresponds to the $M_L = 0$ in Fig. 3. Similar nodal patterns can be observed in the nodal patterns of the four frontier π-MOs of **5a** [16]. Once the alignment of the nodal planes has been clearly defined the effect of different structural perturbations can be readily conceptualized on a qualitative basis through a consideration of the relative size of the MO coefficients on each atom on the perimeter

Table 1. Key parameters predicted for the major spectral bands in the TD-DFT and ZINDO/s calculations of **5a**, **5b** and **5g**–**5i**

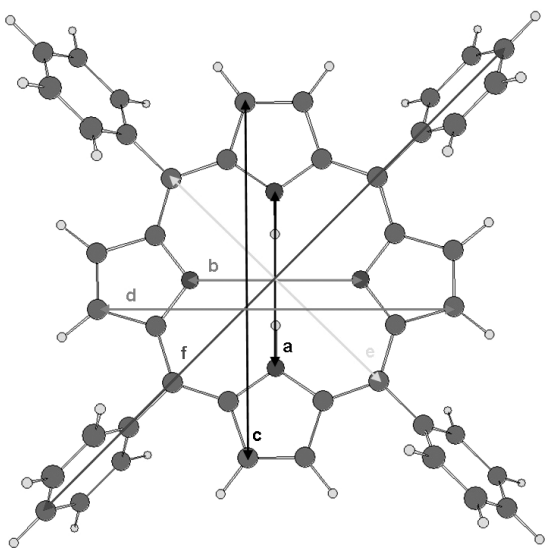

	a	b	c	d	e	f
P	4.22	4.08	8.52	8.52	6.88	—
TPP	4.24	4.06	8.50	8.53	6.93	15.56
TPhen	4.19	4.09	8.36	8.32	6.80	—
5a	4.16	4.09	6.90	6.87	6.75	15.36
5b	4.16	4.11	6.81	6.78	6.72	15.36
5c	4.15	4.10	6.81	6.80	6.72	15.29
5d	4.15	4.10	6.81	6.80	6.72	15.29
5e	4.15	4.10	6.81	6.80	6.72	15.28
5g	4.19	4.10	6.79	6.80	6.72	15.31
5h	4.10	4.20	6.77	7.01	6.73	15.37
5i	4.24	4.14	6.79	6.74	6.73	15.40

since the deep saddling of the ligand is determined primarily by the steric crowding caused by the fused phenanthrene ring moieties and the aryl groups on the *meso*-carbons. Michl's perimeter model [18] can be used to rationalize how different peripheral fused rings affect the HOMO–LUMO band gap and the ΔHOMO and ΔLUMO values, and hence the spectral properties (Fig. 3). The effect of adding fused rings to the periphery of the porphyrin ligand can be readily understood with reference to the effect of the symmetry lowering structural perturbations on the relative energies of four key frontier π-MOs primarily associated with the 16 atom 18 π-electron cyclic polyene on the inner ligand perimeter. The perimeter model approach often enables accurate predictions about key aspects of the electronic structure and optical spectroscopy to be made based on a qualitative consideration of the alignment of the nodal planes of the four frontier π-MOs. Under the D_{2h} symmetry of porphyrin compounds the alignment of the 2N nodal planes of the HOMO level is defined for symmetry reasons by the mirror planes running through the pyrrole nitrogens, and this is used to define the identity of the $M_L = 0$ MO in Fig. 3. Once the alignment of the nodal planes has been defined the effect of various structural perturbations on the MO energies can be readily determined.

The **a** and **s** MOs of porphyrin compounds remain accidentally near degenerate. The net stabilizing effect on the **s** MO due to the increased electronegativity of the four pyrrole nitrogens at nodes of the **a** MO is matched by a stabilizing effect on the **a** MO related to the presence of the four peripheral C_2H_2 bridges at nodes of the **s** MO (Fig. 4). There is a strong bonding interaction between the inner ligand perimeter portion of the **a** MO of and

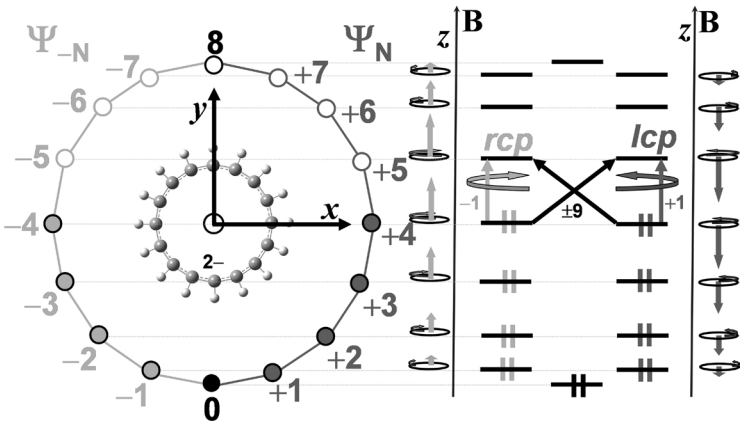

Fig. 3. Michl's perimeter model [18] for $C_{16}H_{16}^{2-}$ (LEFT). The circle represents a diagrammatic representation of the clockwise and counterclockwise motion of π-system electrons on the inner ligand perimeter generating the M_L value for each complex π-MO. The alignment and magnitude of the magnetic moments induced by the electron motion within each π-MO (CENTER) can be predicted based on the right hand rule for solenoids and LCAO calculations. The moments aligned along the *z*-axis with or against the applied field are shown diagrammatically [18]. Right and left handedness is defined within classical optics looking towards the light source of the CD spectrometer (lcp and rcp = left and right circularly polarized light)

what can be viewed as four antibonding ethylene MOs on the ligand periphery. Michl [18] has demonstrated that the effect of the introduction of bridging atoms on the MO energies is determined primarily by the number of atoms in the bridge. When the bridge consists of an even number of atoms the four frontier π-MOs of the parent perimeter are retained as the four frontier π-MOs of the expanded π-system. The size and relative sign phases of the MO coefficients on the perimeter atom where the bridge is attached and the first atom of the bridge determine the ordering of the **a**, **s**, **–a** and **–s** MOs. In the case of metal complexes, symmetry considerations dictate that the **–a** and **–s** MOs remain degenerate, since only the degeneracy of the $M_L = \pm2, \pm4, \pm6$ MOs is lifted on moving from D_{16h} to D_{4h} symmetry (Fig. 4). The introduction of protonated pyrrole nitrogens along the *y*-axis of free base compounds results in a slight lifting of the degeneracy of the LUMO level. In the **–a** and **–s** MOs, the interactions with the peripheral ethylene bridges along the *x*- and *y*-axes are broadly similar, so only a minor lifting of the degeneracy of the LUMO is anticipated based primarily on the relative size of the MO coefficients on the protonated and non-protonated pyrrole nitrogens.

When fused benzene rings are added to the porphyrin ligand in a radially symmetric manner to form tetrabenzoporphyrin (TBP), there is an antibonding interaction between the **a** MO and the C_4H_4 bridge moiety at all eight positions of attachment resulting in a marked destabilization of the MO energy (Figs 4 and 5). In contrast there is a slight stabilization of the **s** MO due to a weak bonding interaction. The energies of the **–a** and **–s** MOs of free base TBP remain largely unchanged because a stabilizing interaction introduced along one axis is balanced by a destabilizing interaction along the other so a low ΔLUMO value is retained. The marked destabilization of the **a** MO leads to a narrowing of the HOMO–LUMO band gap and the introduction of a significant ΔHOMO value, so there is a red shift and intensification of the Q band. Only a relatively minor red shift is observed for the B band due to the interaction between the B and higher energy ππ* states [17]. Radially symmetric fused-ring-expansion of the porphyrin ligand with acenaphthalene moieties to form tetraacenaphthoporphyrin (TANP) has a markedly different effect on the relative energies of the four frontier π-MOs. A destabilization of both the **a** and **s** MOs is anticipated, since there are antibonding interactions between the β-carbons of the pyrrole moieties and the two carbon atoms of the peripheral $C_{10}H_6$ bridging units to which they are attached, but this is relatively minor in magnitude, since the MO coefficients on the fused acenaphthalene rings are relatively low. In contrast, there is a marked stabilization of the **–a** and **–s** MOs since there is a strong bonding interaction along the *y*- and *x*-axis, respectively, involving relatively large MO coefficients. The ΔHOMO value of TANP is therefore significantly lower than that predicted for TBP and there is a markedly narrower HOMO–LUMO band gap. This accounts for the unusually large red shift of the Q and B bands reported by Lash and others [10, 14], and the spectral properties which in other regards are broadly similar to those of the parent porphyrin compound since ΔHOMO ≈ ΔLUMO ≈ 0. A similar pattern is observed when fused phenanthrenes are added to form tetraphenanthroporphyrin (TPhen) but the stabilizations of the **–a** and **–s** MOs are not as large as those observed for TANP so a larger HOMO–LUMO band gap is, therefore, predicted. When phenyl substituents are added at the *meso*-carbons to form tetraphenyltetrabenzoporphyrin (TPTBP), tetraphenyltetraacenaphthoporphyrin (TPTANP) and TPTP there is a destabilization of the **s** MO due to the large coefficients on these atoms, which typically results in a decrease in the ΔHOMO value and the observed Q band intensity and a red shift of both the Q and B bands (Figs 4 and 5). No significant destabilization of the **a** MO is anticipated, since the *meso*-carbons lie on nodal planes. The destabilization of the **s** MO of TPTANP results in a soft MCD chromophore with ΔHOMO ≈ ΔLUMO ≈ 0. A somewhat larger ΔHOMO value is predicted for TPTPs (Fig. 5), resulting in a more pronounced red shift and greater Q band intensity than is observed with TPTANPs [16, 17].

It has long been known that the optical properties of tetraarylporphyrin compounds can be fine-tuned using the Hammett parameter of a *para*-substituent (σ_p) by

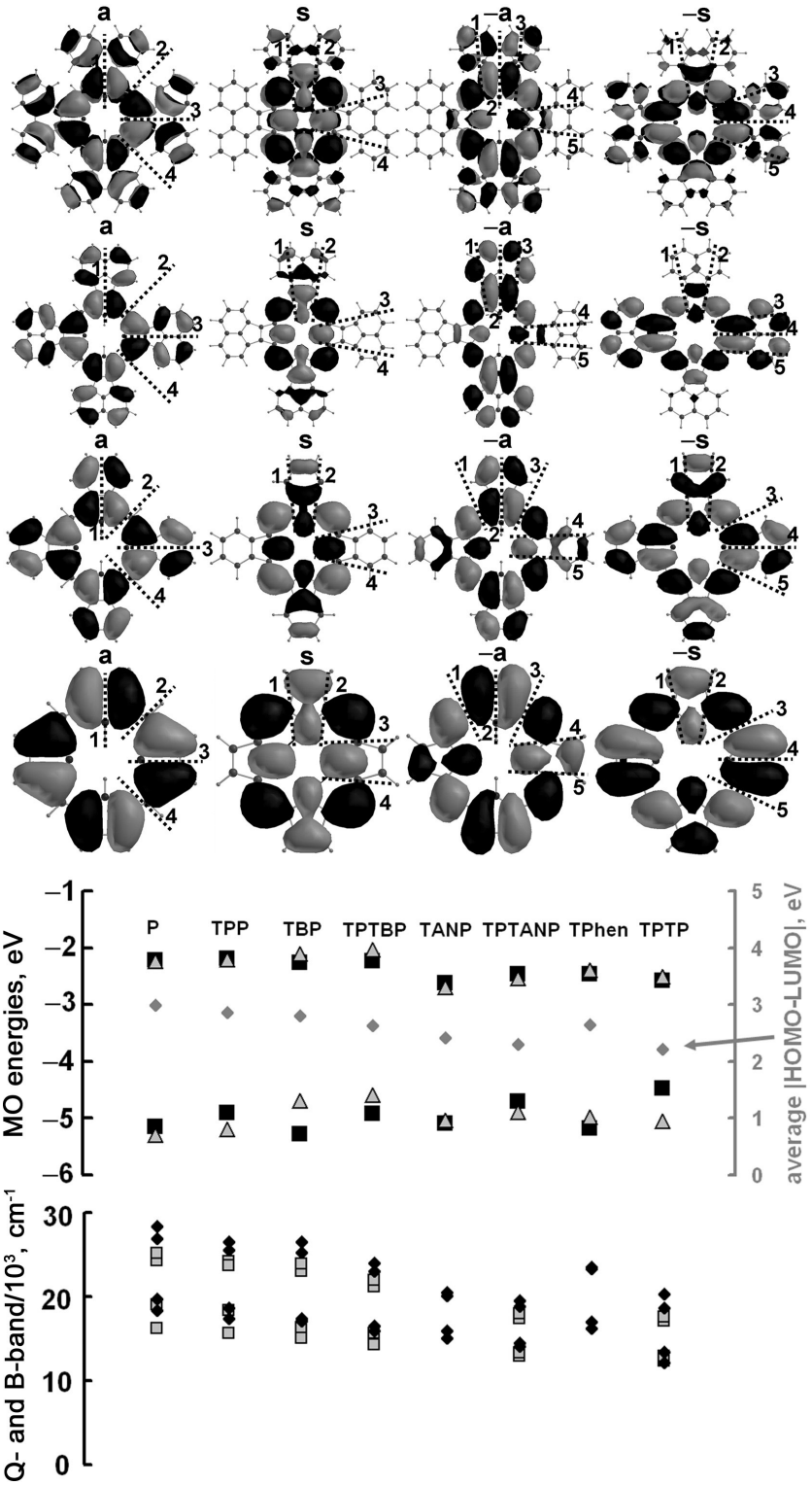

Fig. 4. MO energies of the frontier π-MOs of radially symmetric fused-ring-expanded porphyrinoids in TD-DFT calculations (bottom) carried out with the B3LYP functional using 6-31G(d) basis sets. The **a** and –**a** MOs with nodal planes on the protonated pyrrole nitrogens ($1a_u$ and $1b_{2g}$*) are denoted with light gray triangles, while the **s** and –**s** MOs ($1b_{1u}$ and $1b_{3g}$*) with significant MO coefficients on these atoms are denoted by black squares. The nodal patterns of the **a**, **s**, –**a** and –**s** MOs of, from bottom to top, porphyrin (P), tetrabenzoporphyrin (TBP), tetraacenaphthoporphyrin (TANP), tetraphenanthroporphyrin (TPhen) at an isosurface of 0.01 a.u. (TOP). The imino protons are aligned with the *y*-axis. Gray and black are used to denote the phase changes in the isosurfaces. Similar nodal patterns are observed for the corresponding tetraphenylporphyrinoids [17]. The average HOMO–LUMO band gap values taking into account all four MOs derived from the HOMO and LUMO of the parent perimeter are denoted by dark gray diamonds and are plotted against a secondary axis (CENTER). The trends in the band gap values closely mirror those observed in the experimental (black diamonds) and calculated (light gray squares) energies of the Q and B bands (BOTTOM)

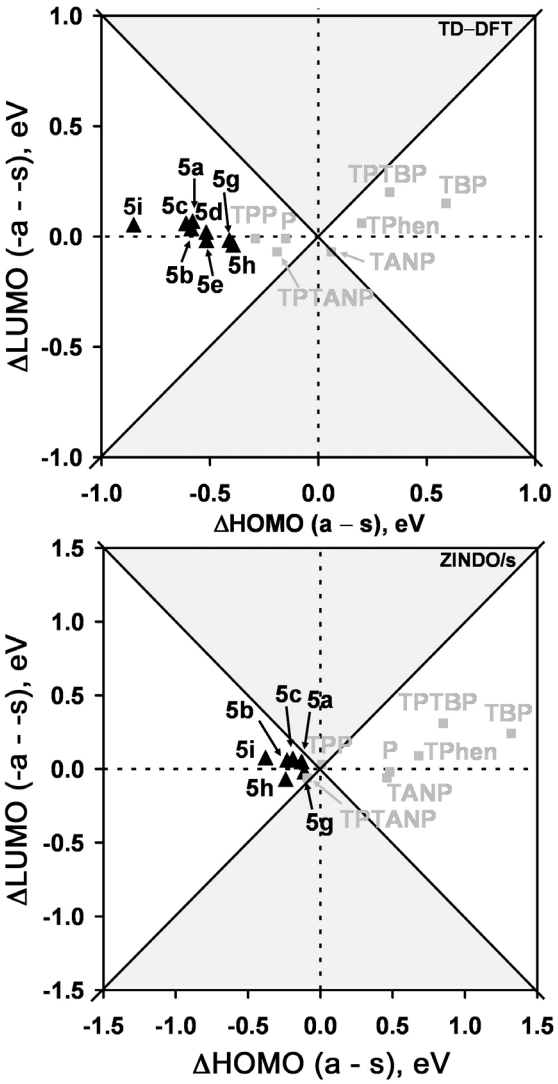

Fig. 5. The effect of structural perturbations on the ΔHOMO and ΔLUMO values predicted by B3LYP (LEFT) and by ZINDO/s (RIGHT) calculations for the same set of B3LYP optimized geometries for **5a**–**5i** and free base porphyrin (P), tetraphenylporphyrin (TPP), tetrabenzoporphyrin (TBP), tetraphenyltetrabenzoporphyrin (TPTBP), tetraacenaphthoporphyrin (TANP), tetraphenyltetraacenaphthoporphyrin (TPTANP), tetraphenanthroporphyrin (TPhen) and tetraphenyltetraphenanthroporphyrin (TPTP). In the light gray shaded areas where ΔLUMO > ΔHOMO a +/– MCD sign sequence is anticipated [17, 18] for the Q band in ascending energy terms, while a –/+ sign sequence is anticipated in the unshaded areas where ΔHOMO > ΔLUMO

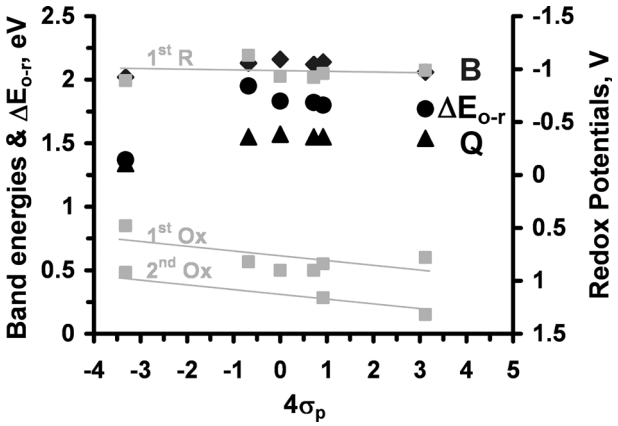

Fig. 6. The observed Q and B band wavelengths and ΔE_{o-r} values in eV are denoted by black triangles, diamonds and circles, respectively, and are plotted *vs*. $4\sigma_p$ [30]. Redox potentials for the oxidation and reduction steps relative to the saturated calomel electrode are plotted as light gray squares against a secondary axis

carrying out the synthesis with different benzaldehydes so that *meso*-aryl groups with strongly electron withdrawing or donating properties are introduced into the π-system. Linear plots can often be obtained for $E_{½}$ *vs*. $4\sigma_p$ for the first and second oxidation and reduction potentials of structurally related porphyrins [27]. For example, in the mid-1970s, Kadish and Morrison [28] reported linear trends in the redox values of free base H_2(*p*-X)TPP compounds with $–OCH_3$, $–CH_3$, –H, –F, $–COOCH_3$, –Cl, –CN and $–NO_2$ substituents. A similar trend was recently reported for H_2(*p*-X) TPTPs [16] (Fig. 6). A particularly large interaction is anticipated in this context, since increased steric hindrance rotates the phenyl groups almost into the plane of the inner perimeter of the π-system (Fig. 1). Kadish and Morrison [28] reported that the closest agreement with the redox value trend was observed with electron accepting substituents, while compounds with electron donating $–CH_3$ and $–NMe_2$ substituents were found to lie off the trendline. When ΔHOMO ≈ ΔLUMO ≈ 0, as is predicted to be the case for TPTPs, and there are close to fully forbidden Q bands and fully allowed B bands based on the $\Delta M_L = \pm 1$ and ±9 properties of the Q and B transitions, it is reasonable to expect that the redox properties of the aryl substituents will modify the energies of both the Q and B bands based on the changes in the separation of the first oxidation and reduction potentials (ΔE_{o-r}), which determine the magnitude of the HOMO–LUMO band gap.

When the energies predicted for the four frontier π-MOs of the H_2(*p*-X)TPTP compounds are plotted (Fig. 7), the energies for the **5i** MOs do not lie on the trend line observed in the energies for the compounds with electron withdrawing substituents, however. This is not surprising, since Kadish and Morrison [28] only reported a correlation between the redox potentials and the σ_p of the substituents for TPPs containing *para*-substituents with electron accepting properties (Fig. 6). Marked differences are observed in the spectra of **5b** and **5i** relative to those of **5a** and **5f** (Fig. 8). In both cases, there is a marked intensification of the Q band region, which may be related in part to increased vibrational band intensity caused by the $–CH_3$ and $–N(CH_3)_2$ groups. An unprecedented red shift of the Q band is observed for **5i** based on the strong electron donating properties

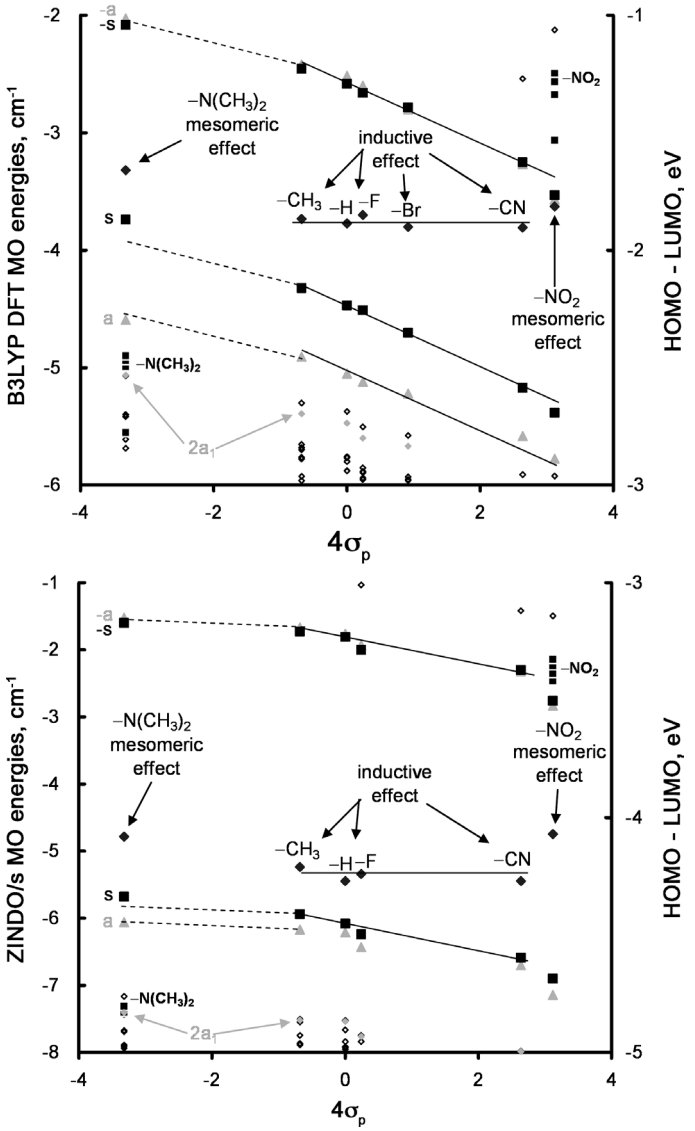

Fig. 7. The energies of the frontier π-MOs predicted by TD-DFT (TOP) and ZINDO/s (BOTTOM) calculations plotted against the Hammett parameter (σ_p) [30]. Black squares denote the **s** and **–s** MOs and large light gray triangles are used for the **a** and **–a** MOs. Small squares denote π-MOs introduced by the *para*-substituents, while open diamonds are used to denote MOs associated with the ligand π-system. Gray diamonds are used to highlight the $2a_1$ MO which has nodal patterns that are similar to those of the **s** MO, which in group theory terms is the $1a_1$ MO. The HOMO–LUMO band gap values are plotted against a right hand axis using large dark gray diamonds with labels denoting the type of *para*-substituent in each case

of the $–N(CH_3)_2$ groups. DFT and INDO/s calculations predict that the introduction of more strongly electron donating groups at the *para*-positions of the phenyl groups, destabilizes the four frontier π-MOs (Fig. 7). As would be anticipated on this basis, negative shifts are observed in both the oxidation and reduction potentials (Fig. 6). The inductive effect associated primarily with σ-bonding is not expected to significantly alter the size of the HOMO–LUMO band gap, since the HOMO and LUMO are destabilized to an equal extent. This pattern is predicted for **5a**–**5g** in B3LYP calculations with 6–31G(d) basis sets (Fig. 7). Michl has demonstrated that when a strong mesomeric effect is introduced, as is the case with the $–NO_2$ groups in **5h** and the $–N(CH_3)_2$ groups in **5i**, the presence of the substituent can have markedly differing effects on the energies of the four frontier π-MOs, based on differing extents of mixing with MOs that are associated primarily with the $2p_z$ AOs on the substituents. Where **5i** is concerned, this mixing is most significant in the **a** and **s** MOs, since they lie closer in energy to the MOs introduced by the substituents [17]. The destabilization which results from this is most marked in the case of the **s** MO due to the large MO coefficients on the *meso*-carbons (Fig. 4), and this causes a decrease in the HOMO–LUMO band gap relative to **5a** and TPP and hence a marked red shift of the Q and B bands (Fig. 8). The increase in the predicted ΔHOMO value is consistent with the marked intensification of the Q(0,0) bands. An electron-withdrawing mesomeric interaction is anticipated for **5h** in which the largest interaction is expected to be with the **–a** and **–s** MOs due to the presence of low-lying unoccupied MOs associated with the substituents. Since these MOs lack the radial symmetry of the **a** and **s** MOs (Fig. 2), a reasonably similar interaction is anticipated. The **–a** and **–s** MOs both have significant MO coefficients at the four *meso*-carbons, so there is less scope for a significant ΔLUMO value.

The results of the TD-DFT calculations for the H_2(*p*-X)TPTP compounds are somewhat problematic (Fig. 8). In the experimental data, a single intense pair of coupled Faraday $\mathcal{B}_0$ terms is consistently observed in the B band region, corresponding to the most intense band in the absorption spectrum. In the calculated TD-DFT spectra, however, the most intense band in the B band region is usually predicted to lie significantly to the blue of the initial set of bands that are associated primarily with the four frontier π-MOs (Fig. 8), due to configurational interaction between the lower energy B state and a state associated primarily with the $2a_1 \rightarrow$ **–s** one-electron transition (Table 2). The $2a_1$ MO has nodal patterns which are similar to those of the **s** MO, which in group theory terms is the $1a_1$ MO. There is an even more marked discrepancy between the calculated and observed spectra of **5h**, where there are low-lying unoccupied MOs associated with the $–NO_2$ substituents (Fig. 7). In contrast in the ZINDO/s spectra calculated using the same set of B3LYP geometries, the bands associated with transitions from the **a** and **s** MOs to the **–a** and **–s** MOs are consistently predicted to be the most intense in the B band region of the spectra. Similar

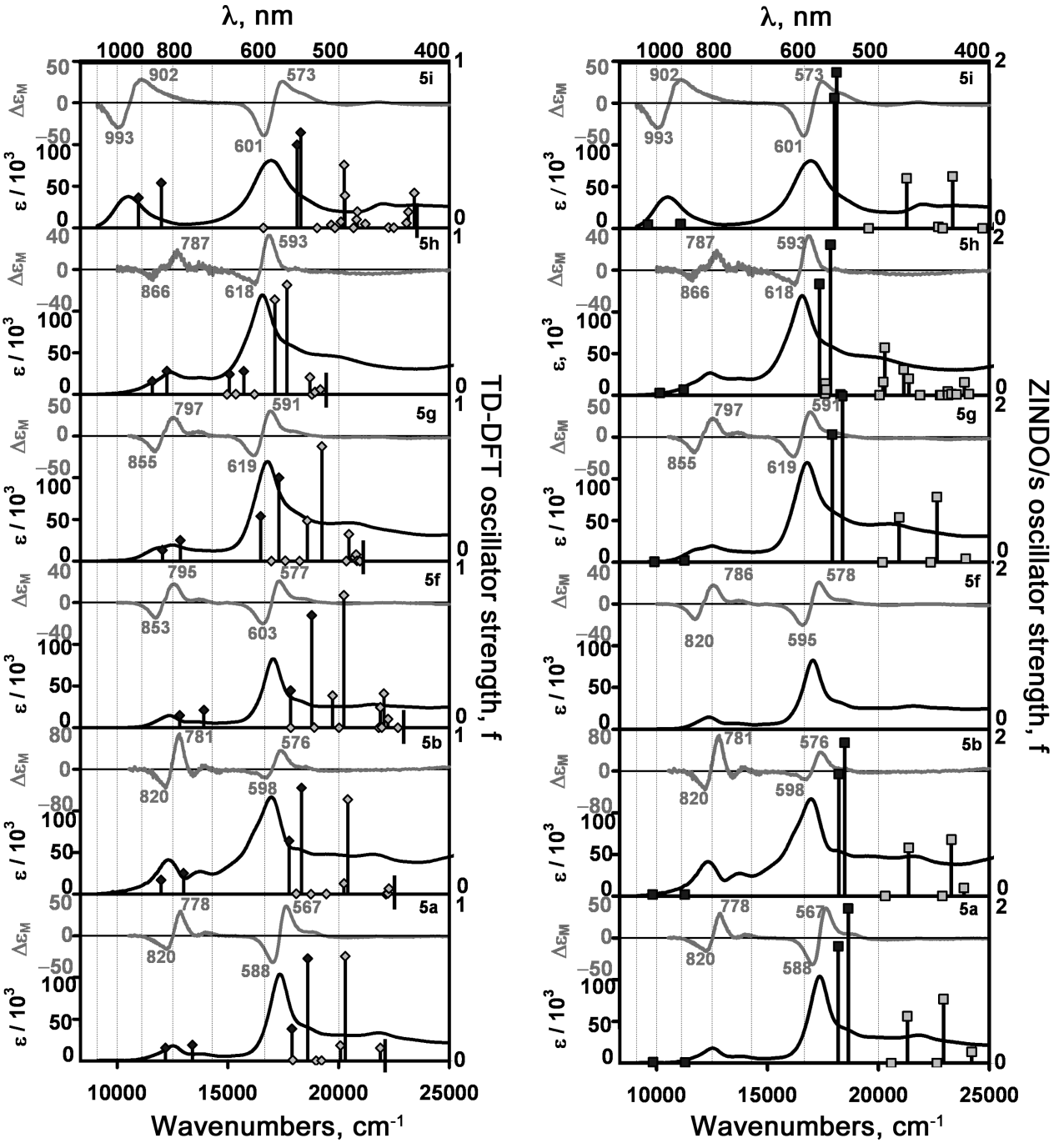

Fig. 8. Absorption and MCD spectra of **5a**, **5b** and **5f**–**5i** recorded in 99:1 (v/v) $CHCl_3$:ethanol in $CHCl_3$ at 298 K. The coupled pairs of overlapping Faraday $\mathcal{B}_0$ terms associated with the Q and B bands can be viewed as pseudo-$\mathcal{A}_1$ terms arising from transitions into close lying excited states that would be orbitally degenerate if a central metal were present. TD-DFT (LEFT) and ZINDO/s (RIGHT) spectra are plotted against a right hand axis using green diamonds and blue squares, respectively. The Q and B bands associated primarily with one-electron transitions between the **a**, **s**, –**a** and –**s** MOs are highlighted with black diamonds and light gray squares

issues have been encountered in the calculated spectra of other porphyrinoids [16, 17]. For example, two intense bands are predicted in the UV region of D_{4h} symmetry metal porphyrin complexes, while only one intense $\mathcal{A}_1$ term is typically observed in the experimental spectra. Nemykin has demonstrated that the size of the Hartree Fock component added to the exchange-correlation functional to form hybrid functionals such as B3LYP has a significant effect on the relative energies of the highest lying occupied MOs in calculations carried out on phthalocyanines and that this can have a significant effect on the calculated spectra [29]. The separation of the $1a_1$ and $2a_1$ MOs is significantly larger within the ZINDO/s calculation (Fig. 7), and there are smaller ΔHOMO values so there is less configurational interaction between the Q and B and higher ππ* states (Table 2).

Table 2. Key parameters predicted for the major spectral bands in the TD-DFT and ZINDO/s calculations of **5a**, **5b** and **5g**–**5i**.

	Band[b]	Obs.[c]	TD-DFT[a]						ZINDO/s[a]					
			Calcd.[d]	Percentage contributions[e]					Calcd.[d]	Percentage contributions[e]				
			nm (f)	**a** → **–a**	**a** → **–s**	**s** → **–a**	**s** → **–s**	$2a_1$ → **–s**	nm (f)	**a** → **–a**	**a** → **–s**	**s** → **–a**	**s** → **–s**	$2a_1$ → **–s**
	Q_x	820	821 (0.08)	20	0	0	73	0	1016 (0.01)	39	0	0	54	0
	Q_y	778	747 (0.10)	0	25	66	0	0	885 (0.01)	0	48	46	0	0
5a	B_x	588	559 (0.19)	49	0	0	2	34	550 (1.40)	50	0	0	33	8
	B_y	567	538 (0.61)	0	58	9	0	0	537 (1.85)	0	45	46	0	0
	$\pi\pi^*_x$	—	492 (0.63)	19	0	0	4	54	436 (0.77)	4	0	0	6	66
	Q_x	820	821 (0.08)	21	0	0	73	0	1017 (0.02)	36	0	0	56	0
	Q_y	781	747 (0.10)	0	23	68	0	0	887 (0.02)	0	45	49	0	0
5b	B_x	598	559 (0.19)	57	0	0	4	23	549 (1.46)	53	0	0	32	7
	B_y	576	538 (0.61)	0	62	8	0	0	541 (1.84)	0	47	44	0	0
	$\pi\pi^*_x$	—	493 (0.63)	12	0	0	3	68	429 (0.68)	3	0	0	5	67
	Q_x	855	830 (0.06)	26	0	0	71	0	1010 (0.01)	42	0	0	50	0
	Q_y	797	778 (0.13)	0	26	66	0	0	888 (0.02)	0	46	48	0	0
5g	B_x	619	607 (0.29)	50	0	0	6	29	558 (1.53)	47	0	0	36	8
	B_y	591	578 (0.50)	0	53	9	0	0	544 (1.99)	0	46	44	0	0
	$\pi\pi^*_x$	—	520 (0.69)	13	0	0	5	61	442 (0.78)	4	0	0	6	67
	Q_x	866	863 (0.08)	19	0	0	73	0	986 (0.03)	31	0	0	45	0
	Q_y	767	817 (0.14)	0	20	69	0	0	892 (0.07)	0	32	49	0	0
5h	B_y	618	663 (0.12)	53	0	0	3	33	577 (1.33)	0	37	30	0	11
	B_x	593	636 (0.14)	0	43	3	0	0	560 (1.80)	39	0	0	35	0
	$\pi\pi^*_x$	—	566 (0.66)	17	0	0	6	51	493 (0.57)	0	0	0	12	40
	Q_x	902	913 (0.18)	19	0	0	73	0	1040 (0.05)	32	0	0	60	0
	Q_y	834	834 (0.27)	0	13	72	0	0	902 (0.05)	0	41	53	0	0
5i	B_y	601	552 (0.50)	70	0	0	2	10	555 (1.56)	0	57	29	0	3
	B_x	573	547 (0.57)	0	73	4	0	0	552 (1.87)	51	0	0	39	0
	$\pi\pi^*_x$	—	493 (0.38)	6	0	0	0	81	428 (0.62)	2	0	0	4	35

[a] Details are provided for TD-DFT and ZINDO/s calculations of **5a**, **5b** and **5g**–**5i** carried out using the same set of B3LYP geometries. [b]The band assignment is described in the text. [c]The wavelengths of the band centers of the Faraday $\mathcal{B}_0$ terms observed for the Q(0,0) and B(0,0) bands in the MCD spectra of **5a**, **5b** and **5g**–**5i**. [d] The calculated wavelength of the Q and B bands and the most intense ππ* band to the red of the B bands with the oscillator strengths provided in parentheses. The data are arranged in five labeled rows for each compound. [e]The predicted percentage contribution from each one-electron transition between the four frontier π-MOs derived from the HOMO and LUMO of the parent $C_{16}H_{16}^{2-}$ perimeter and the one-electron transition between the $2a_1$ MO of the ligand π-system and the **–s** MO.

CONCLUSION

Michl's perimeter model provides a conceptual framework which can be readily used to analyze and predict trends observed in experimental and calculated optical spectra. The red shifts observed for the Q bands of tetraphenyltetraphenanthro- and tetraphenyltetraacenaphthoporphyrin compounds are due primarily to the marked stabilizations of the **–a** and **–s** MOs relative to the electronic structure of TPP. The retention of OAM properties similar to those of the parent perimeter (ΔHOMO ≈ ΔLUMO ≈ 0) is an important factor where the B band is concerned since this limits the amount of configurational interaction with higher energy ππ* states. Further marked modifications of the HOMO–LUMO band gap are predicted when *para*-substituents are introduced to the phenyl groups on the *meso*-carbons, which have a strong mesomeric effect. In contrast, when the inductive effect is the dominant factor as is the case with **5a**–**5g**, the energies of the **a**, **s**, **–a** and **–s** MOs are predicted to be modified to a similar extent by the electron withdrawing or donating properties

of the *para*-substituents of the aryl groups. The TD-DFT calculations of TPTPs appear to be problematic due to an overestimation of the degree of configurational interaction between one of the B excited state and a higher lying $\pi\pi^*$ states. This provides further evidence that the results of TD-DFT calculations can not be lined up uncritically against the experimental spectra and that detailed studies of trends in the MCD spectra and TD-DFT spectra of structurally related porphyrinoids are often required to definitively assign the major bands within the optical spectra.

Acknowledgements

This work was supported by the Department of Science and Technology (DST), Japan and the National Research Foundation (NRF), South Africa through a DST/NRF Chairs Initiative for Professor of Medicinal Chemistry and Nanotechnology, the National Natural Science Foundation of China (No. 20971066 to Z.S.), National Basic Research Program of China (No. 2011CB808704 to Z.S.) and a Grant-in-Aid for Scientific Research from the Ministry of Education, Culture, Sports, Science and Technology, Japan (No. 20108007 (π-space) to N.K.)

REFERENCES

1. a) Bonnett R. *Chem. Soc. Rev.* 1995; **24**: 19–33. b) Zhang Z, Ferrence GM and Lash TD. *Org. Lett.* 2009; **11**: 1249–1252. c) Lu T, Shao P, Mathew I, Sand A and Sun W. *J. Am. Chem. Soc.* 2008; **130**: 15782–15783. d) Comuzzi C, Cogoi S, Overhand M, Van der Marel GA, Overkleeft HS and Xodo LE. *J. Med. Chem.* 2006; **49**: 196–204. e) Drobizhev M, Stepanenko Y, Dzenis Y, Karotki A, Rebane A, Taylor PN and Anderson HL. *J. Phys. Chem. B* 2005; **109**: 7223–7236.
2. a) Ikeda C, Sakamoto N and Nabeshima T. *Org. Lett.* 2008; **10**: 4601–4604. b) Wu D, Descalzo AB, Weik F, Emmerling F, Shen Z, You X-Z and Rurack K. *Angew. Chem. Int. Ed.* 2008; **47**: 193–197. c) Zhu X-J, Fu S-T, Wong W-K, Guo J-P and Wong W-Y. *Angew. Chem. Int. Ed.* 2006; **45**: 3150–3154.
3. a) Lim JM, Yoon ZS, Shin J-Y, Kim KS, Yoon M-C and Kim D. *Chem. Commun.* 2009; 261–273. b) Kim KS, Yoon ZS, Ricks AB, Shin J-Y, Mori S, Sankar J, Saito S, Jung YM, Wasielewski MR, Osuka A and Kim D. *J. Phys. Chem. A* 2009; **113**: 4498–4506. c) Yoon ZS, Cho D-G, Kim KS, Sessler JL and Kim D. *J. Am. Chem. Soc.* 2008; **130**: 6930–6931.
4. Calvete M, Yang GY and Hanack M. *Synth. Met.* 2004; **141**: 231–243.
5. a) Holten D, Bocian DF and Lindsey JS. *Acc. Chem. Res.* 2002; **35**: 57–69. b) He X, Liu H, Li Y, Liu Y, Lu F, Li Y and Zhu D. *Macromol. Chem. Phys.* 2005; **206**: 2199–2205. c) Iqbal R, Moratti SC, Holmes AB, Yahioglu G, Milgrom LR, Cacialli F, Morgado J and Friend RH. *J. Mater. Sci.* 2000; **11**: 97–103. d) Wagner RW, Lindsey JS, Seth J, Palaniappan V and Bocian DF. *J. Am. Chem. Soc.* 1996; **118**: 3996–3997.
6. a) Wu D, Shen Z, Xue Z-L and You X-Z. Chin J. *Inorg. Chem.* 2007; **23**: 1–14. b) Elemans JAAW, Van Hameren R, Nolte RJM and Rowan AE, *Adv. Mater.* 2006: **18**: 1251–1266. c) Hsieh C-P, Lu H-P, Chiu C-L, Lee C-W, Chuang S-H, Mai C-L, Yen W-N, Hsu S-J, Diau EW-G and Yeh C-Y. *J. Mater. Chem.* 2010; **20**: 1127–1134. d) Hayashi S, Tanaka M, Hayashi H, Eu S, Umeyama T, Matano Y, Araki Y and Imahori H. *J. Phys. Chem. C* 2008; **112**: 15576–15585.
7. a) Maretina IA. *Russ. J. Gen. Chem.* 2009; **79**: 1544–1581. b) Anderson HL. *Chem. Commun.* 1999; 2323–2330. c) Zou H, Therien MJ and Blasie JK. *J. Phys. Chem. B* 2008; **112**: 1350–1357. d) Winters MU, Karnbratt J, Eng M, Wilson CJ, Anderson HL and Albinsson B. *J. Phys. Chem. C* 2007; **111**: 7192–7199. e) Shen Z, Uno H, Shimizu Y and Ono N. *Org. Biomol. Chem.* 2004; **2**: 3442–3447. f) Kuebler SM, Denning RG and Anderson HL. *J. Am. Chem. Soc.* 2000; **122**: 339–347. g) Taylor PN, Wylie AP, Huuskonen J and Anderson HL. *Angew. Chem. Int. Ed.* 1998; **37**: 986–989.
8. a) Misra R and Chandrashekar TK. *Acc. Chem. Res.* 2008; **41**: 265–279. b) Sessler JL and Seidel D. *Angew. Chem. Int. Ed.* 2003; **42**: 5134–5175. c) Reddy JS and Anand VG. *J. Am. Chem. Soc.* 2009; **131**: 15433–15439. d) Kamimura Y, Shimizu S and Osuka A. *Chem. Eur. J.* 2007: **13**: 1620–1628. e) Inokuma Y, Matsunari T, Ono N, Uno H and Osuka A. *Angew. Chem. Int. Ed.* 2005; **44**: 1856–1860.
9. a) Tokuji S, Yurino T, Aratani N, Shinokubo H and Osuka A. *Chem. Eur. J.* 2009; **15**: 12208–12211. b) Siczek M and Chmielewski PJ. *Angew. Chem. Int. Ed.* 2007; **46**: 7432–7436. c) Uno H, Kitawaki Y and Ono N. *Chem. Commun.* 2002; 116–117. d) Ogawa T, Nishimoto Y, Yoshida N, Ono N and Osuka A. *Angew. Chem. Int. Ed.* 1999; **38**: 176–179.
10. a) Lash TD. *J. Porphyrins Phthalocyanines* 2001: **5**: 267–288. b) Lash TD. In *The Porphyrin Handbook*, Vol. 2, Kadish KM, Smith KM and Guilard R. (Eds.) Academic Press: San Diego, 1999; Chapter 10, pp 125–199.
11. Davis NKS, Pawlicki M and Anderson HL. *Org. Lett.* 2008; **10**: 3945–3947. b) Manley JM, Roper TJ and Lash TD. *J. Org. Chem.* 2005; **70**: 874–891. c) Ono N, Yamamoto T, Shimada N, Kuroki K, Wada M, Utsunomiya R, Yano T, Uno H and Murashima T, *Heterocycles* 2003; **61**: 433–447.
12. Haddad RE, Gazeau S, Pecaut J, Marchon J, Medforth CJ and Shelnutt JA. *J. Am. Chem. Soc.* 2003; **125**: 1253–1268.
13. Shelnutt JA, Song X-Z, Ma J-G, Jia S-L, Jentzen W and Medforth CJ. *Chem. Soc. Rev.* 1998; **27**: 31–41.

14. Spence JD and Lash TD. *J. Org. Chem.* 2000; **65**: 1530–1539.
15. Xu H-J, Shen Z, Okujima T, Ono N and You X-Z. *Tetrahedron Lett.* 2006; **47**: 931–934.
16. Xu H-J, Mack J, Descalzo AB, Shen Z and Kobayashi N, You X-Z and Rurack K. *Chem. Eur. J.* 2011; **17**: 8965–8983.
17. Mack J, Asano Y, Kobayashi N and Stillman MJ. *J. Am. Chem. Soc.* 2005; **127**: 17697–17711.
18. Michl J. *J. Am. Chem. Soc.* 1978; **100**: 6801–6811. b) Michl J. *Tetrahedron* 1984; **40**: 3845–3934.
19. Gouterman M. In *The Porphyrins*, Vol. 3, Dolphin D. (Ed.) Academic Press: New York, 1978; pp 1–165.
20. Mack J, Bunya M, Shimizu Y, Uoyama H, Komobuchi N, Okujima T, Uno H, Ito S, Stillman MJ, Ono N and Kobayashi N. *Chem. Eur. J.* 2008; **14**: 5001–5020.
21. Fukuda T, Homma S and Kobayashi N. *Chem. Eur. J.* 2005; **11**: 5205–5216.
22. Gaussian 03, Revision C.02, Frisch MJ, Trucks GW, Schlegel HB, Scuseria GE, Robb MA, Cheeseman JR, Montgomery Jr. JA, Vreven T, Kudin KN, Burant JC, Millam JM, Iyengar SS, Tomasi J, Barone V, Mennucci B, Cossi M, Scalmani G, Rega N, Petersson GA, Nakatsuji H, Hada M, Ehara M, Toyota K, Fukuda R, Hasegawa J, Ishida M, Nakajima T, Honda Y, Kitao O, Nakai H, Klene M, Li X, Knox JE, Hratchian HP, Cross JB, Bakken V, Adamo C, Jaramillo J, Gomperts R, Stratmann RE, Yazyev O, Austin AJ, Cammi R, Pomelli C, Ochterski JW, Ayala PY, Morokuma K, Voth GA, Salvador P, Dannenberg JJ, Zakrzewski VG, Dapprich S, Daniels AD, Strain MC, Farkas O, Malick DK, Rabuck AD, Raghavachari K, Foresman JB, Ortiz JV, Cui Q, Baboul AG, Clifford S, Cioslowski J, Stefanov BB, Liu G, Liashenko A, Piskorz P, Komaromi I, Martin RL, Fox DJ, Keith T, Al-Laham MA, Peng CY, Nanayakkara A, Challacombe M, Gill PMW, Johnson B, Chen W, Wong MW, Gonzalez C and Pople JA. Gaussian, Inc., Wallingford CT, 2004.
23. Mack J, Stillman MJ and Kobayashi N. *Coord. Chem. Rev.* 2007; **251**: 429–453.
24. a) Moffitt WJ. *J. Chem. Phys.* 1954; **22**: 320–333. b) Moffitt WJ. *J. Chem. Phys.* 1954; **22**: 1820–1829.
25. a) Mack J and Stillman MJ. In *The Porphyrin Handbook*, Vol. 16, Kadish K, Smith K and Guilard R. (Eds.) Academic Press: New York, 2003; Chapter 103, pp 43–116. b) Mack J and Stillman MJ. *Coord. Chem Rev.* 2001; **219–221**: 993–1032.
26. Perrin MH. *J. Chem. Phys.* 1973; **59**: 2090–2104.
27. Kadish KM, Van Caemelbecke E and Royal G. In *The Porphyrin Handbook*, Vol. 8, Kadish KM, Smith KM and Guilard R. (Eds.) Academic Press: New York, 1999; Chapter 55, pp 1–114.
28. Kadish KM and Morrison MM. *J. Am. Chem. Soc.* 1976; **98**: 3326–3328.
29. Nemykin VN, Hadt RG, Belusludov RV, Mizuseki H and Kawazoe Y. *J. Phys. Chem. A* 2007; **111**: 12901–12913.
30. Hansch C, Leo A and Taft RW. *Chem. Rev.* 1991; **91**: 165–195.